Available online at www.sciencedirect.com
SCIENCE DIRECT®
Journal of Power Sources 144 (2005) 42–53
JOURNAL OF POWER SOURCES
www.elsevier.com/locate/jpowsour

Modeling the influence of GDL and flow-field plate parameters on the reaction distribution in the PEMFC cathode catalyst layer

Wei Sun[a,b], Brant A. Peppley[b,c], Kunal Karan[a,b,*]

[a] *Department of Chemical Engineering, Queen's University, Kingston, Ont., Canada K7L 3N6*
[b] *Fuel Cell Research Center, Queen's University, Kingston, Ont., Canada K7L 3N6*
[c] *Department of Chemistry and Chemical Engineering, The Royal Military College of Canada, Kingston, Ont., Canada*

Received 10 November 2004; accepted 26 November 2004
Available online 15 January 2005

Abstract

In this paper, a two-dimensional cross-the-channel model was applied to investigate the influence of gas diffusion layer (GDL) property and flow-field geometry on the local reaction rate in the PEMFC cathode catalyst layer. The model predictions show that the rate of consumption of oxygen or current density under the land area may differ considerably from that under the channel. Simulation results indicate that for a fixed channel width, increasing the channel-to-land width ratio results in improved water transport and positively impacts the overall reaction rates at high overpotential. However, too high ratio may retard electron transport and thus lead to worse cathode performance. Numerical simulation results revealed that GDL electrical conductivity and thickness have a strong influence on how the chemical species and electrons are transported to the active catalyst sites. Depending on the electrical conductivity of GDL, the region of higher reaction rate may occur either under the land or under the channel. Consideration of orthotropic electrical conductivity of GDL affects the simulation results significantly highlighting the need to improve our understanding of GDL transport coefficients. Simulation of GDL compression effects showed that the total current density is not affected significantly but current density distribution is. The extent of reactant bypass through the GDL from one channel to the other depends on the GDL permeability and results in a significant enhancement in reaction rates.

Keywords: PEMFC cathode; Flow-field plate; Gas diffusion layer; Reaction distribution; PEMFC modeling

1. Introduction

PEMFCs have been actively researched for a number of years because of their advantages such as low-temperature operation, rapid start-up and high power density [1]. There is a continued interest in improving the understanding of various physico-electro-chemical processes occurring in a PEMFC. Of particular interest are the cathode processes which account for a majority of the total cell electrochemical losses.

The electrochemical reaction occurring at the cathode of PEMFC involves three different species – ions (protons), electrons, and chemical species (oxygen and water). These electrochemical reactions occur in a thin catalyst layer, which is in contact with a proton-conducting membrane on one side and a porous gas diffusion layer (GDL) on the other side. At the cathode side, the GDL allows the transport of the reactant oxygen and electrons from the flow-field channel and from under the flow-field land, respectively, to reaction sites. In addition, the GDL allows removal of water produced in the catalyst layer. From the schematic depiction of the PEMFC cathode in Fig. 1, it can be readily seen that the pathways for electron and species transport from the flow-field plate to the catalyst layer are different. The local electrochemical reaction rate in the catalyst layer is, therefore, influenced by the geometric parameters and transport properties of both the GDL and the flow-field plate. Mathematical modeling may

* Corresponding author. Tel.: +1 613 533 3095; fax: +1 613 533 6637.
E-mail address: karan@chee.queensu.ca (K. Karan).

0378-7753/$ – see front matter © 2004 Elsevier B.V. All rights reserved.
doi:10.1016/j.jpowsour.2004.11.035

provide useful insights into how these parameters can influence catalyst layer performance.

Over the past 20 years, a wide variety of PEMFC models of varying complexity have been developed. These include 1-D models [2–7] and 2-D along-the-channel (ATC) models [8–14] and, more recently reported, 3-D models [15–19]. A detailed review of PEMFC models has been published by our group [20]. A 2-D cross-the-channel (CTC) model by West and Fuller [21] was applied to analyze the influence of the bipolar plate rib or land on local reaction rate. However, in their model the catalyst layer was treated as an ultra-thin layer, and electron transport in the cathode was not included. In fact, a majority of the 1-D, 2-D and 3-D models treat the catalyst layer to be a thin-layer or a fully flooded thin-layer [22–23]. Models where the catalyst layer is treated in the most detail are agglomerate-type models [24–32], wherein the catalyst layer is considered as a domain comprising agglomerates of catalyst particles. However, a majority of the agglomerate models are 1-D, an exception being 2-D ATC models [31–32]. In summary, owing to the directions considered in the 1-D and 2-D ATC models or because of the description of the catalyst layer as a thin-film, the influence of flow-field plate geometry on the variation of the local electrochemical reaction rate has not been reported.

The objective of this paper is to investigate the influence of flow-field and GDL geometric parameters and transport properties on the local electrochemical reaction rate distribution in the PEMFC cathode catalyst layer. The catalyst layer is modeled as spherical-agglomerates of catalyst-electrolyte providing detailed distribution of the reaction rate.

2. Model description

A detailed description of the model employed in this paper is provided elsewhere [33–34]. Here we only briefly describe the computational geometry and key equations, boundary conditions, model assumptions, computational procedure and input parameters.

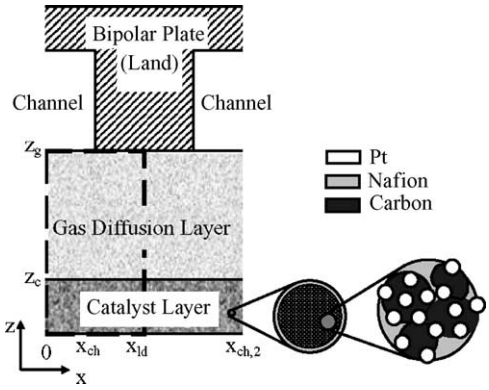

Fig. 1. Schematic of a PEMFC cathode with an agglomerate structure catalyst layer.

2.1. Computational geometry

Fig. 1 illustrates the cathode structure of a typical PEMFC, in which the catalyst layer is composed of many agglomerates. An agglomerate is made up of platinum particles, carbon black and Nafion. Each agglomerate is covered by a thin film of electrolyte. Assuming symmetry in adjacent parallel channels a domain consisting of a half-channel and a half land is considered for the base case. The rectangle defined by dashed line describes the region of interest. When reactant bypass phenomenon from channel-to-channel is modeled, the computational geometry extends to $x = x_{ch,2}$. Chemical species transport is assumed to occur by the sequential pathways – diffusion through gas pores in GDL and catalyst layer, followed by diffusion of dissolved oxygen within the agglomerate [32].

2.2. Key Model equations

2.2.1. Reactant transport

Chemical species transport in the GDL and the catalyst layer is described by the Maxwell–Stefan equations [35]. The diffusivities in the GDL and catalyst layer were modified through the Bruggemann relation [2,4]:

$$\nabla \cdot n_i = \nabla \cdot \left[-\rho w_i \sum_j D_{ij}^{\text{eff}} \frac{M}{M_j} \left(\nabla w_j + w_j \frac{\nabla M}{M} \right) \right] \quad (1)$$

$$D_{ij}^{\text{eff}} = D_{ij} \varepsilon_{\text{GDL}}^{1.5} \quad (2)$$

$$D_{ij,\text{C}}^{\text{eff}} = D_{ij} \varepsilon_{\text{CAT}}^{1.5} \quad (3)$$

where, n_i is species mass flux vector, w_i is mass fraction for component i, ρ is gas mixture density, M is molecular weight of the gas mixture, D_{ij} is binary diffusivities of species i and j, ε is porosity.

Using Bruggeman correlation for the catalyst layer is probably appropriate because it was originally derived for granular packing. However, its application to the fibrous GDL may be questionable. This topic is being further investigated in our research group [36].

2.2.2. Electrode reaction

The gaseous oxygen must first dissolve and then diffuse through the electrolyte film surrounding the agglomerate, prior to participating in the reaction or diffusing inward in the agglomerate while reacting. The overall reaction rate for oxygen consumption in the cathode can be expressed in terms of the local oxygen concentration, reaction rate constant, an effectiveness factor for the electrode reaction, E_r, and agglomerate physical parameters.

$$R_{O_2} = \frac{P_{O_2}}{H} \left(\frac{1}{E_r k_c (1 - \varepsilon_{\text{CAT}})} + \frac{(r_{\text{agg}} + \delta)\delta}{a_{\text{agg}} r_{\text{agg}} D} \right)^{-1} \quad (4)$$

where, R_{O_2} is oxygen reaction rate based on catalyst layer volume, H is Henry's law constant, E_r is the catalyst effectiveness factor, r_{agg} is the agglomerate radius, δ is the thickness of the electrolyte film covering an agglomerate, D is the dissolved oxygen diffusivity in Nafion. In our model, the charge-transfer reaction is considered to be the rate-limiting step in the oxygen reduction reaction (ORR) [37]. Accordingly, the electrochemical reaction rate constant (k_c) is given by the following equation:

$$k_c = \left(\frac{\varepsilon_l m_{Pt} S_{ac}}{4Ft_{cl}(1-\varepsilon_{CAT})}\right)\left[\frac{i_0^{ref}}{C_{O_2}^{ref}}\right]\left[\exp\left(-\frac{\alpha_c F}{RT}\eta\right) - \exp\left(\frac{(1-\alpha_c)F}{RT}\eta\right)\right] \quad (5)$$

The catalyst effectiveness factor for the spherical agglomerate is given by [38]

$$E_r = \frac{1}{\Phi_L}\left(\frac{1}{\tanh(3\Phi_L)} - \frac{1}{3\Phi_L}\right) \quad (6)$$

where Φ_L is a dimensionless group, commonly known as Thiele's modulus for chemical reactions:

$$\Phi_L = \frac{r_{agg}}{3}\sqrt{\frac{k_c}{D_{eff}}} \quad (7)$$

where, D_{eff} is the effective diffusivity of the dissolved oxygen in electrolyte phase.

In the catalyst layer, under electrical load conditions the protons are continuously consumed generating current. According to the species conservation, the divergence of current density would be related oxygen reaction rate:

$$\nabla \cdot i = 4F\frac{P_{O_2}}{H}\left(\frac{1}{E_r k_c(1-\varepsilon_{CAT})} + \frac{(r_{agg}+\delta)\delta}{a_{agg} r_{agg} D}\right)^{-1} \quad (8)$$

2.2.3. Charge transport

Proton migration and electron transport in the cathode can be described by Ohm's law:

$$i_P = -k_l^{eff}\nabla\phi_l \quad (9)$$

$$i_{e,C} = -k_s^{eff}\nabla\phi_s \quad (10)$$

where, i_P is the proton flux and $i_{e,C}$ is the electron flow in the catalyst layer, k_l and k_s are proton conductivity and electron conductivity, respectively. ϕ_l is the potential in electrolyte phase, and ϕ_s is the electrical potential in electron transport.

Conservation of the charge leads to the following equations:

$$\text{in the catalyst layer}: \quad \nabla \cdot i_P + \nabla \cdot i = 0 \quad (11)$$

$$\text{in the GDL}: \quad \nabla \cdot i_{e,G} = 0 \quad (12)$$

where, $i_{e,G}$ is the electron flow in the GDL.

Only the cathode is considered in this model. The potential losses in the cathode include activation overpotential at the cathode, electronic losses in both the GDL and the catalyst layer, ionic loss in the catalyst layer. Thus, the total potential loss is defined as the nominal cathode overpotential (NCO), which is the potential difference between the electron phase at the land ($z = z_g$ in Fig. 1) and the electrolyte phase at the interface between catalyst layer and membrane ($z = 0$ in Fig. 1). This definition of overpotential holds true because the electron phase potential at $z = z_g$ is considered to be constant and equal to zero. However, it must be noted that the strict definition of overpotential is the difference in potential of the two phases at zero current and that at any current.

2.3. Boundary conditions

The computational sub-domains (SDs) and associated dimensions are shown in the Fig. 2, which is used to define boundary conditions. The normal fluxes of any transported parameter, Φ, which may represent species flux, proton flux and electron flux, are assumed to be zero at $x = 0$ and $x = x_{ld}$, because symmetry is assumed at these boundaries.

$$(\Phi) \cdot n = 0 \quad (13)$$

where, $\cdot n$ is normal flux operator.

2.3.1. Boundary conditions for chemical species transport (Eq. (1))

$$x_i = x_{i,o} \quad \text{at } z = z_g,\ 0 \le x \le x_{ch}: \quad (14)$$

$$(n_i) \cdot n = 0 \quad \text{at } z = z_g,\ x_{ch} < x \le x_{ld} \text{ and } z = 0: \quad (15)$$

2.3.2. Boundary conditions for proton charge balance (Eq. (9))

$$(i_P) \cdot n = 0 \quad \text{at } z = z_c: \quad (16)$$

$$\phi_l = \phi_{l,o} \quad \text{at } z = 0: \quad (17)$$

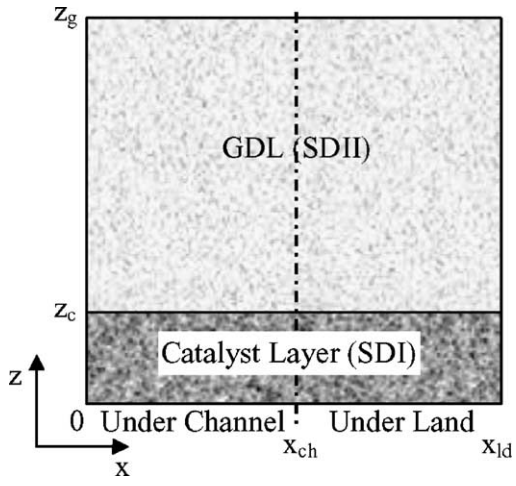

Fig. 2. Sub-domains of simulation.

Table 1
Operating and electrode parameters for base case

Parameters	Value	Units	Sources
Operating pressure (absolute)	1.5	atm	
Operating temperature	80	°C	
Oxygen/nitrogen ratio	21/79	–	
Air feed relative humidity	50%	–	
Half channel width	0.5	mm	
Half channel land width	0.5	mm	
GDL thickness	250	μm	
Porosity of GDL, ε_{GDL}	0.4	–	
Pt loading, m_{Pt}	0.4	mg cm^{-2}	
Pt particle diameter, r_{Pt}	2.5	nm	
Effective specific agglomerate surface area, a_{agg}	3.6×10^5	m^2 m^{-3}	
Radius of agglomerate, r_{agg}	1	μm	
Catalyst layer thickness, t_{cl}	15	μm	[28]
Porosity of catalyst layer, ε_{CAT}	0.1	–	[32]
Conductivity of GDL, k_s	100	S m^{-1}	[25]
Cathodic transfer coefficient[a], α_c			
Low slope (≥0.8 V)	1	–	[50]
High slope (<0.8 V)	0.61	–	
Reference exchange current density[a], i_0^{ref}			
Low slope (≥0.8 V)	3.85×10^{-8}	A cm^{-2}	[50]
High slope (<0.8 V)	1.5×10^{-6}	A cm^{-2}	
O_2 diffusivity in Nafion[a], D	8.45×10^{-10}	m^2 s^{-1}	[50]
Henry's constant[a], H	0.3125	atm m^3 mol^{-1}	[37]
Thickness of electrolyte film covering each agglomerate, δ	80	nm	[40]
Electrolyte fraction in agglomerate, ε_{agg}	0.5	–	[14]
Reference O_2 concentration[b], $C_{O_2}^{ref}$	0.85	mol m^{-3}	[50]
Effective Pt surface ratio, ε_l	0.75	–	[51]
Binary diffusivities			
PD_{O_2,H_2O}	3.70×10^{-5}	atm m^2 s^{-1}	
PD_{O_2,N_2}	2.79×10^{-5}	atm m^2 s^{-1}	[52]
PD_{N_2,H_2O}	3.87×10^{-5}	atm m^2 s^{-1}	

[a] 80 °C.
[b] 80 °C and 1.5 atm air.

2.3.3. Boundary conditions for electron charge balance (Eq. (10))

$$\phi_s = 0 \quad \text{at } z = z_g,\ x_{ch} < x \le x_{ld}: \tag{18}$$

$$(i_{e,C}) \cdot n = 0 \quad \text{at } z = 0: \tag{19}$$

2.4. Model assumptions

The key assumptions employed in the model are as follows:

- isothermal and steady state operation;
- partial pressure losses in the electrode are only caused by multi-component diffusion;
- agglomerates are spherical in shape, mono-dispersed, and evenly distributed;
- local overpotential within an agglomerate is assumed to be constant.

2.5. Solution procedure

The model equations combined with boundary conditions listed in the prior sections were solved with the finite element method using the commercially available PDE solver program FEMLAB®. The stationary non-linear solver option, which is used for non-linear stationary PDE problems, was chosen to solve the highly non-linear problem. Of three different solution forms available, as recommended in FEMLAB user's guide [39], the general solution form was chosen for the non-linear problem.

2.6. Model parameters

The operating conditions and electrode parameters are shown in Table 1.

3. Results and discussions

Fig. 3 shows the cathode polarization curve generated by our model for the base case. The cathode potential shown in Fig. 3 is obtained by subtracting the nominal cathode overpotential (NCO) from the theoretical oxygen reduction potential. The NCO includes cathode activation overpotential electronic losses in the GDL and the catalyst layer as well as

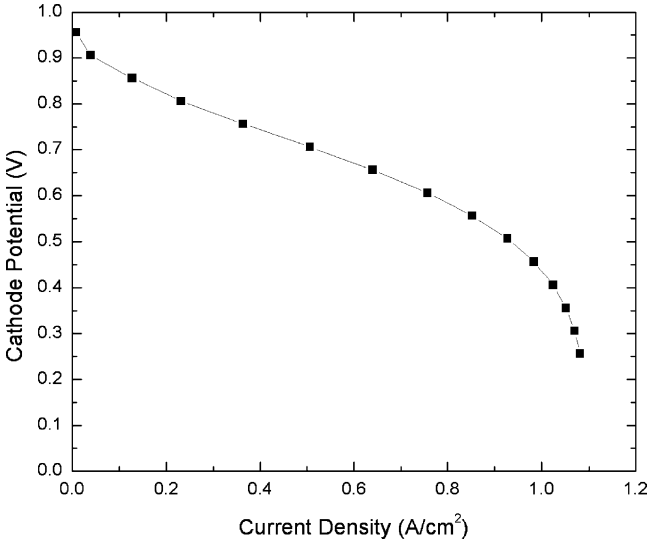

Fig. 3. Cathode polarization curve of base case.

proton transport losses in the electrolyte phase of the catalyst layer.

$$V = E_{\text{th}} - \text{NCO} \tag{20}$$

where,

$$E_{\text{th}} = 1.229 - 8.456 \times 10^{-4}(T - 298.15) + 4.31 \times 10^{-5} T \left(\ln[P_{\text{H}_2}] + \frac{1}{2} \ln[P_{\text{O}_2}] \right) \tag{21}$$

The cathode polarization curve of Fig. 3 does not include the potential losses due to membrane resistance, anode overpotentials and electrical contact resistance. The polarization curve follows the general trend observed in typical experimental results [22,40–43].

3.1. Effect of channel-to-land width ratio on current density

One of the key flow-field plate design parameters is the channel-to-land ratio. Whereas a wider channel may promote chemical species transport, a corresponding thinner land width may restrict electron transport. Because the electrochemical reaction involves both the chemical species and electrons, the nature and extent of how the channel-to-land (Ch-Ld) ratio affects the cathode performance will depend on the competing effect of oxygen and electron transport.

To investigate the effect of flow-field geometric parameters, simulations were carried out for three Ch-Ld ratios. In all cases, the channel width was kept constant while the land width was varied. Current density distributions at $z = 0$ for three Ch-Ld ratios at NCOs of 0.4, 0.5 and 0.6 V, are shown in Fig. 4. In the figure, average current density at the catalyst layer/membrane interface ($z = 0$), i_{avg}, represents the total

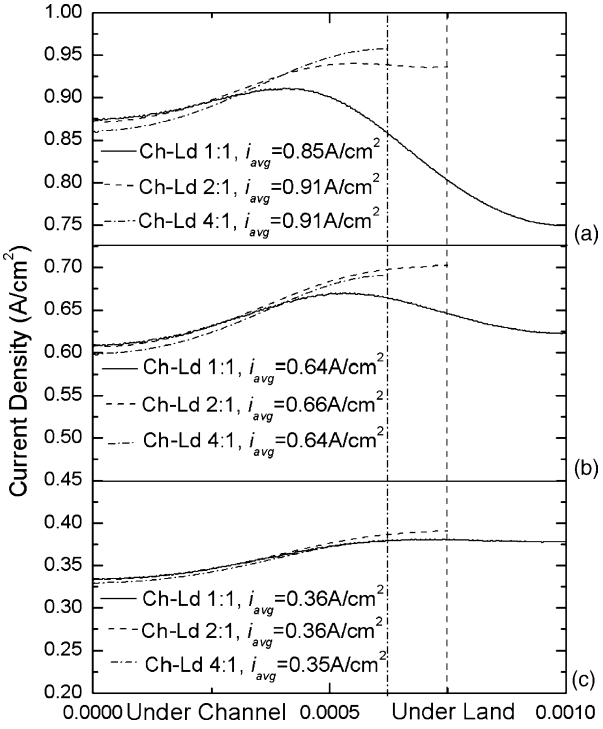

Fig. 4. Current density distributions at $z = 0$ for three Ch-Ld ratios: 1:1, 2:1 and 4:1 for (a) high, (b) intermediate and (c) low NCOs.

current density that is associated with the net reaction rate in the whole catalyst layer.

At low NCO (case c), an increase in Ch-Ld ratio does not improve the cathode performance. Low NCO corresponds to low current density or low oxygen consumption rate. Under these conditions, it appears that electron transport in the cathode has a stronger influence on the electrochemical reaction rate, so increases in channel width, which might be expected to enhance oxygen transport, do not have any significant impact on cathode performance. At high NCO (case a), because the oxygen consumption rate is high, species transport limitations are expected to become important. The simulation results show that at high NCO, an increase in Ch-Ld ratio results in an improvement in the cathode performance. This may be explained by the fact that at high NCO, there is high current density or high oxygen consumption rate. Thus, oxygen transport from the channel to the catalyst layer becomes a dominant factor. By increasing the channel-land ratio, oxygen transport to the region under the land is facilitated. For the case where Ch-Ld equals 2:1, the average current density increased by 7% compared to the base case. Further reduction in land width does not improve cathode performance. For the case of Ch-Ld ratio of 4:1, the current density is actually slightly lower than that for the case Ch-Ld = 2:1. This may be attributed to the increase in resistance to electron transport caused by supplying electrons to a larger region by a thinner land. This translates into reduction in local overpotential in the catalyst area underneath the channel, thereby, a reduction in the electrode reaction rate.

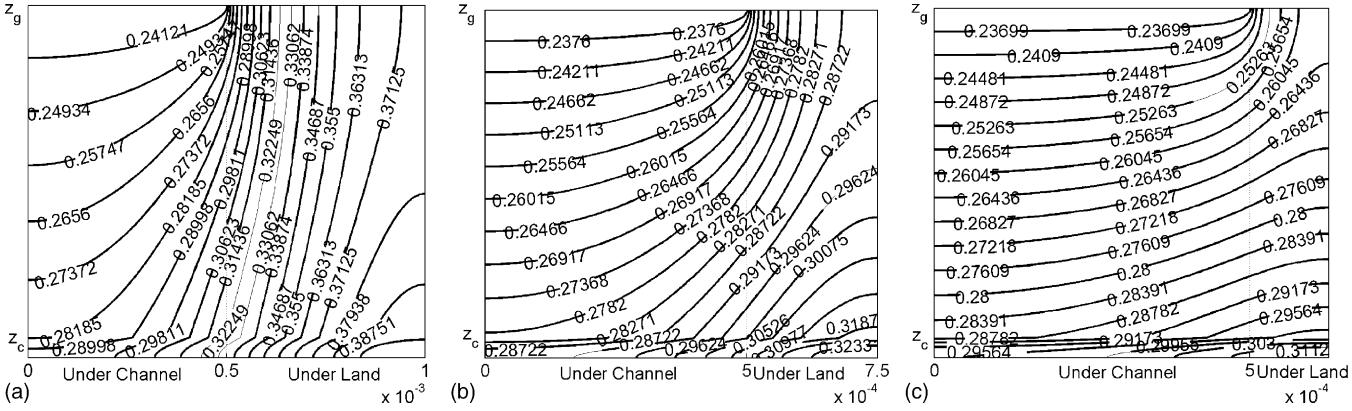

Fig. 5. Water vapour partial pressure (atm) distribution in cathode for three Ch-Ld ratios: (a) 1:1, (b) 2:1 and (c) 4:1. NCO = 0.5 V.

3.2. Effect of channel-to-land width ratio on water transport

A high Ch-Ld ratio is expected to enhance water transport rates and improve water removal from catalyst region under the channel thereby reducing the risk of flooding the catalyst layer. This phenomenon was investigated by studying the water partial pressure distributions in the cathode for the three width ratios. Fig. 5 shows water vapor pressure distribution in cathode for a NCO equal to 0.5 V. It can be seen in the Fig. 5 that the water partial pressure in the cathode decreases significantly with a reduction in the land width. Lower water partial pressure can be a result of either a less amount of water being produced or more effective water removal. In Fig. 4b, the current density under the land area for Ch-Ld ratio of 1:1 is lower than that for Ch-Ld ratios of 2:1 and 4:1 (and therefore the water production rate is lower), i.e. less water is produced under the land due to the cathode reaction. However, as shown in Fig. 5, the water vapour pressure under the land area for a Ch-Ld ratio of 1:1 is higher than that for the other two cases indicating, as expected, thus a low Ch-Ld ratio impairs water removal.

It should be noted that in the preceding discussion, any potential impact of increased contact resistance between the GDL and the flow-field plates as the land width is reduced has not been accounted for. The impact of the effect of the contact resistance is currently being investigated in our laboratory.

3.3. Effect of GDL thickness on current density

Commercial GDL layers are available in variety of thicknesses. To investigate the effect of GDL thickness, simulations were carried out for three GDL thicknesses: 0.15, 0.25 and 0.35 mm. Fig. 6 presents current density distributions at the catalyst layer/membrane interface (e.g. $z = 0$) for three different NCOs. Average current densities are also reported in the figure. Intuitively, one might think that a thinner GDL will be beneficial to the electrode performance, because it would reduce resistance to the transport of both oxygen and electrons. However, simulation results indicate that the average current density is not affected significantly as GDL thickness is reduced from 0.350 to 0.15 mm.

In general, increasing the GDL thickness has the effect of flattening the current density profile across the channel and land area. However, the effect of GDL thickness on local reaction rate (current density) is complicated and depends on the competing effects of oxygen and electron transport. At low overpotential, electron transport plays a more important role in determining the local reaction rate. For the case of 0.15 mm thick GDL, electrons must travel more than three times the

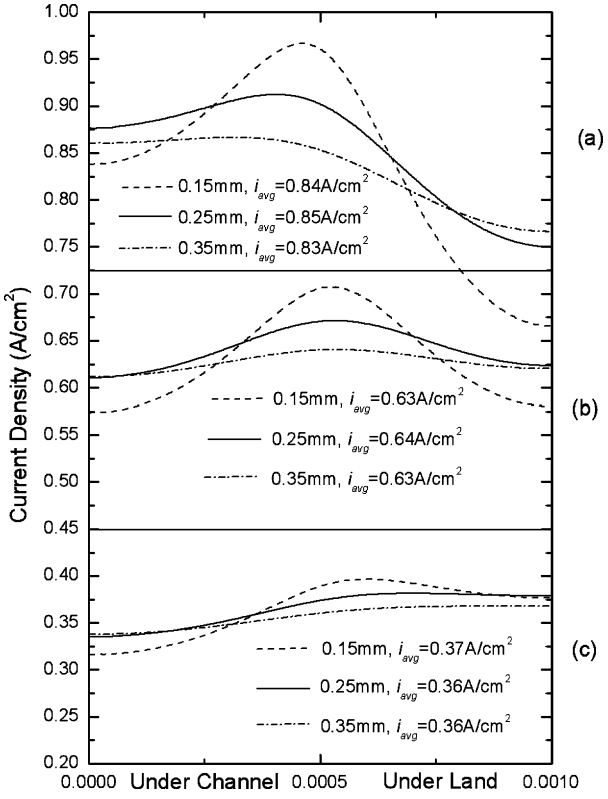

Fig. 6. Current density distributions at $z = 0$ for different GDL thicknesses: 0.15, 0.25 and 0.35 mm for (a) high, (b) moderate and (c) low NCOs, respectively.

distance from current collector edge to a catalyst site at the middle of flow channel compared to a catalyst site located directly underneath the current collector. This indicates that fewer electrons will participate in the electrode reaction in the region under the channel. From the Fig. 6c it can be seen that in the middle of the channel area ($x = 0$), current density decreases with the reduction of the GDL thickness. At higher current density, shown in the Fig. 6a, a similar situation occurs. At this condition, oxygen diffusion is an important rate-limiting factor. Similar to low current density situation, the path for transport of oxygen under the land area is much larger than that under channel area. As a result, in the middle of land region ($x = 1$ mm) the current density decreases with the reduction of the GDL thickness. In summary, the current density distribution depends on the competitive effect between oxygen diffusion and electron transport.

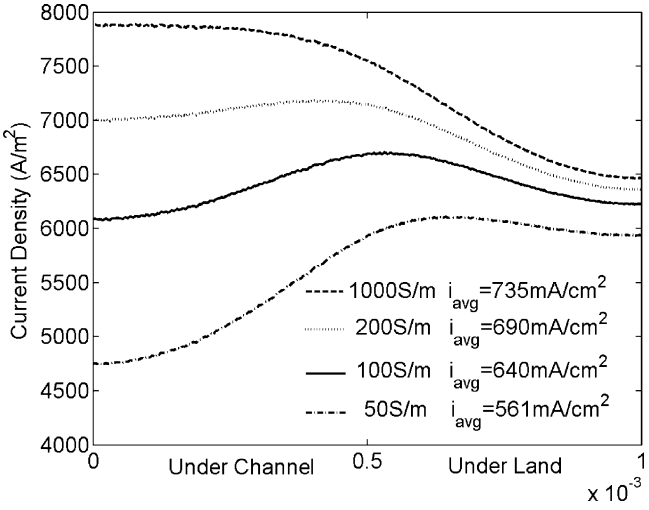

Fig. 8. Current density distribution at $z = 0$ for different GDL conductivities. NCO = 0.5 V.

3.4. Effect of GDL conductivity

A wide range of GDL conductivity values have been employed in PEMFC models [3,17,44–45]. To study the effect of GDL conductivity on the cathode reaction, simulations were carried out for GDL conductivities of 50, 200 and 1000 S m^{-1}, in addition to the base case condition of 100 S m^{-1}. The electron conductivity in the catalyst layer was assumed to be 100 S m^{-1} for all the cases [53]. Fig. 7 depicts the local overpotential distributions in the catalyst layer for the four different GDL conductivities at NCO = 0.5 V. For the case where the GDL conductivity is 50 S m^{-1}, the local overpotential varies up to 20% from the minimum to the maximum. This will cause a considerable difference in the prediction of local current density, which cannot be captured by ultra-thin catalyst layer models, where only a constant overpotential is used.

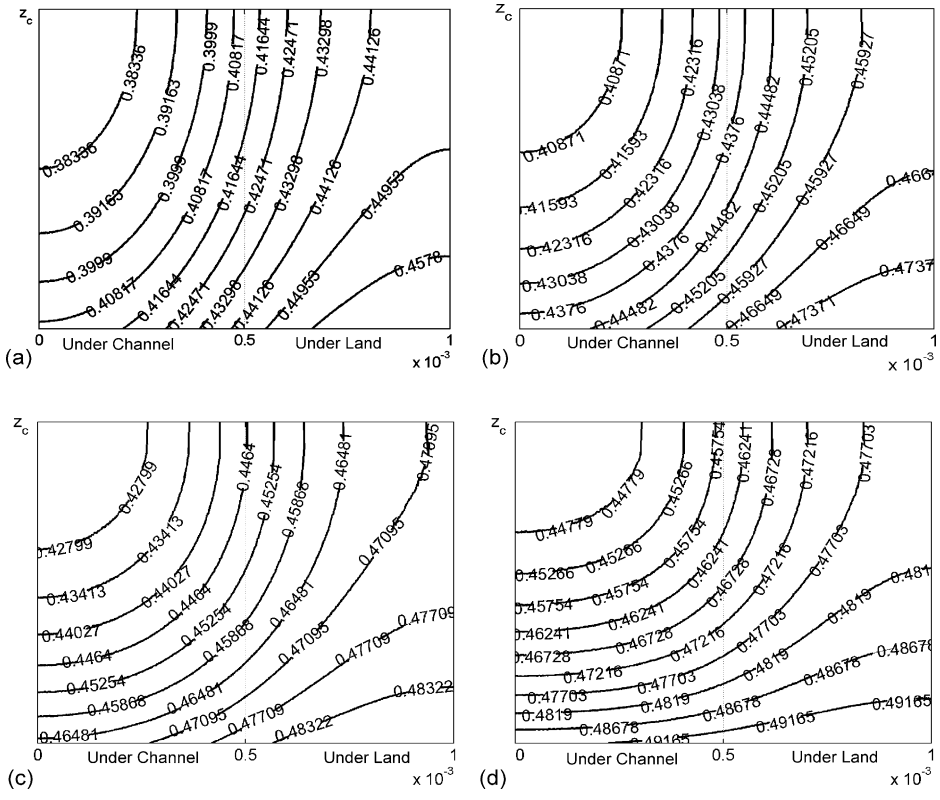

Fig. 7. Local overpotential (V) distributions in the catalyst layer for different GDL conductivities: (a) 50 S m^{-1}, (b) 100 S m^{-1}, (c) 200 S m^{-1} and (d) 1000 S m^{-1}. NCO = 0.5 V.

It should also be noted that for a GDL conductivity of 1000 S m^{-1}, although the electron transport resistance may be negligible, the local overpotentials may still have 10% differential locally. This suggests that proton transport resistance in the catalyst layer also contributes to lower local overpotential.

Fig. 8 illustrates the current density distributions at $z = 0$ for different GDL conductivities at a NCO of 0.5 V. It can be seen that GDL conductivity has a significant impact on current density prediction. With an increase in GDL conductivity from 50 to 1000 S m^{-1}, the predicted current density increases by over 30%. This clearly demonstrates the need of

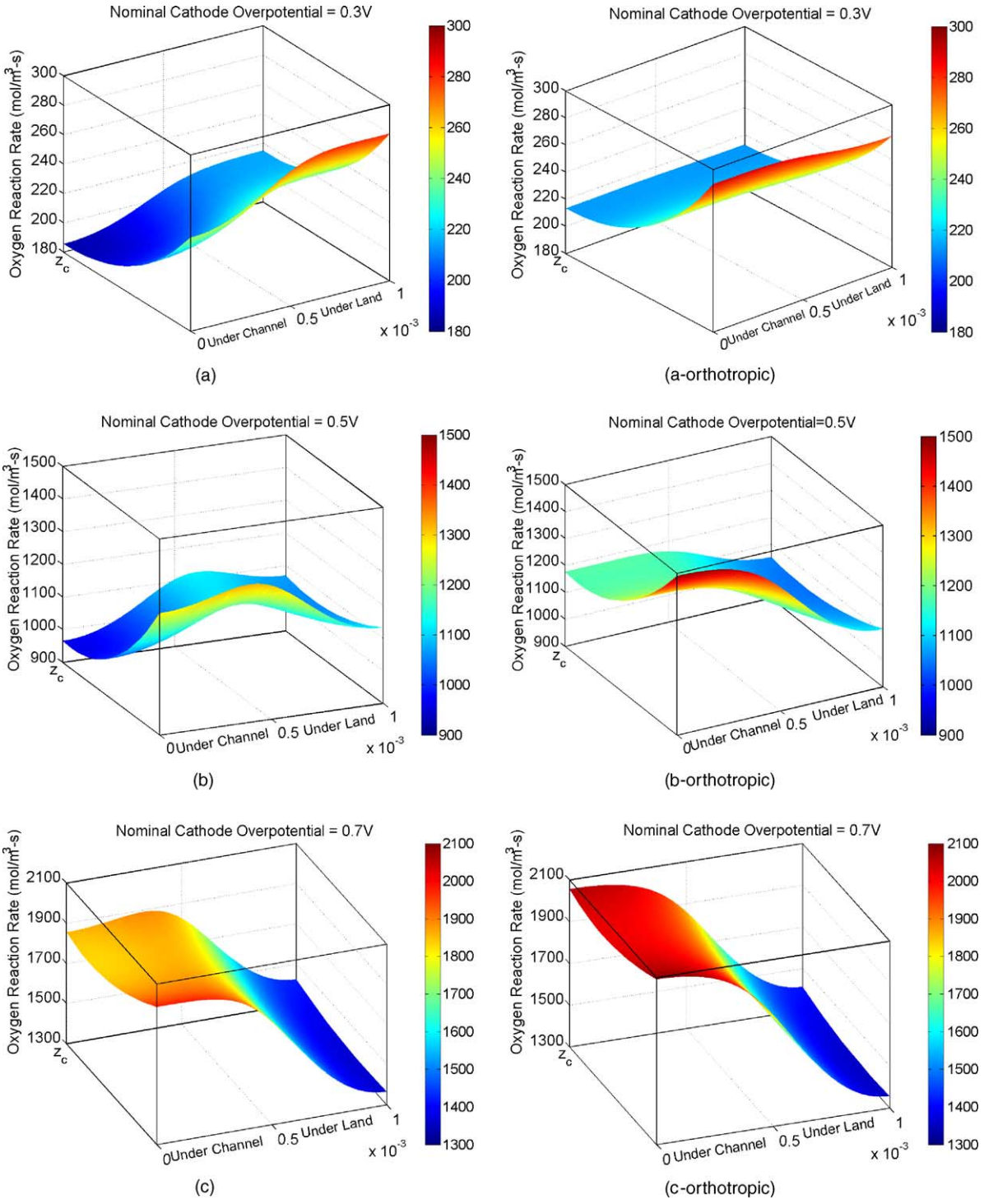

Fig. 9. Oxygen reaction rate distributions in the catalyst layer for base case (isotropic conductivity) and orthotropic GDL conductivity for three NCOs: (a) 0.3 V, (b) 0.5 V and (c) 0.7 V.

selecting an appropriate value for the GDL conductivity if a reliable, predictive model is to be developed.

In addition, GDL conductivity influences the current density distribution. The predicted current density distribution shown in Fig. 8 shows that with an increase in GDL conductivity, there is a significant increase in the current density produced in the catalyst region underneath the channel area and a modest increase in the current density produced below the land area.

3.5. Influence of orthotropic GDL conductivity on reaction rate distribution

The most commonly used GDL materials – carbon paper and carbon cloth – are fibrous by nature and expected to possess conductivities that are different in the in-plane direction compared to the through-plane direction. For certain GDL materials, such as Toray carbon paper, in-plane conductivity has been reported to be more than ten times higher than through-plane conductivity [46]. The two-dimensional across-the-channel model was used to investigate the impact of the orthotropic variation of GDL electrical conductivity. For the simulation, the through-plane conductivity was kept the same as the base case, and the in-plane conductivity was assumed to be 10 times that of the base case value. Fig. 9 shows the comparison of oxygen reaction rate distributions for the base case (isotropic conductivity) and orthotropic GDL conductivity case. A number of interesting observations can be made.

For low NCO (0.3 V) or low reaction rate conditions, it can be observed that for the isotropic case the reaction rate varies significantly in both directions – across the width and along the thickness of the catalyst layer. The oxygen consumption rate is higher underneath the land than that under the channel. For the orthotropic case, the reaction rate varies primarily along the thickness. This is expected because for the orthotropic case high in-plane conductivity leads to a relatively uniform overpotential distribution in the catalyst layer. The rate of consumption is low enough so that oxygen diffusion does not influence the reaction rate distribution across the width. For both cases, more reaction is predicted to occur near the catalyst layer/membrane interface than that near the catalyst layer/GDL interface.

For intermediate NCO (0.5 V), the reaction rate varies significantly in both directions – across the width and through the thickness – of the catalyst layer both the iso- and orthotropic cases. For the isotropic case, at any location along the catalyst thickness, i.e., at a fixed z, the region of higher reaction rate is predicted to be near the channel–land interface. For the orthotropic case, the region of higher reaction rate is predicted to be always underneath the channel at any fixed z. This indicates that when the in-plane conductivity is high oxygen diffusion becomes the limiting process for the electrochemical reaction. At both intermediate and low NCO conditions, the rate of oxygen reduction is greater at the catalyst layer/membrane interface compared to at the catalyst layer/GDL interface for both the iso- and orthotropic cases.

Interestingly, for a high NCO (0.7 V) the reaction rate distribution appears to be very similar both the iso- and orthotropic cases. Further, the reaction rate is predicted to vary primarily across the channel and the land, i.e., the x direction. The reaction rate variation through the depth of the catalyst layer, i.e., the z direction is small. Thus, unlike the lower NCO conditions, the rate of oxygen consumption is no longer considerably higher near the catalyst layer/membrane interface.

3.6. GDL compression effect

In an assembled fuel cell stack, the GDL thickness varies depending on the location. Usually, the portion under land will be compressed by approximately 15% [47]. This compression will probably affect the electronic conductivity and the chemical species transport. A simulation was conducted to investigate how local variation of conductivity and porosity in the GDL caused by compression might affect the local oxygen consumption rate and, hence, the current density.

For the simulation, the GDL under land area was assumed to be 15% thinner than that under the channel area (see Fig. 10). As a result of compression, the porosity and electronic conductivity of the GDL under the land region were assumed to decrease and increase by 15%, respectively with respect to the base case values. The change in binary diffusivities due to porosity change was accounted for by Eq. (2).

Fig. 11 illustrates the current density distribution at $z = 0$ for the base case and with GDL compression. It can be seen

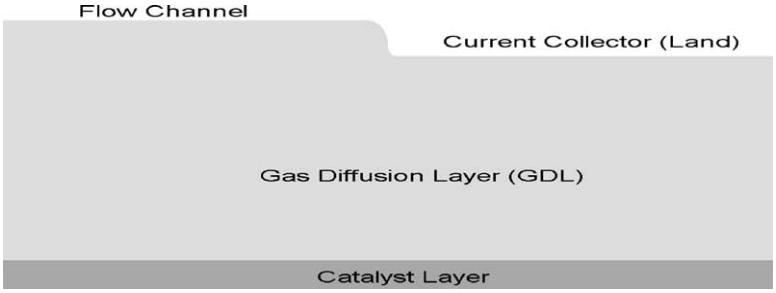

Fig. 10. Cathode structure with compressed GDL.

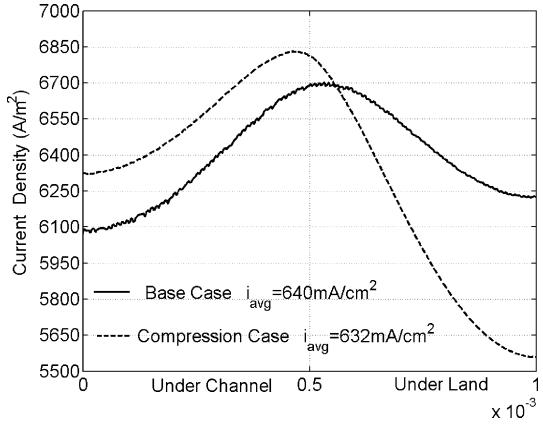

Fig. 11. Current density distributions at $z = 0$ for base case and GDL compression case. NCO = 0.5 V.

that for a 15% increase in conductivity and a 15% decrease in porosity the overall cathode performance is not affected significantly. The fact that the two simultaneous changes appear to have a very small net effect may be because the oxygen reaction rate is determined by two key factors – local oxygen concentration and local overpotential. A compressed GDL increases the resistance to oxygen diffusion to the region under land, resulting in a lower local oxygen concentration. However, at the same time compression increases the local conductivity and it becomes easier to transport electrons to the region under the land, thus increasing local overpotential. Therefore, one effect appears to be balanced by the other. The compression effect, however, may become more important in a situation where a stack is over-compressed or there is variability in humidification resulting in the GDL being deformed with a concentration loss in species transport and no compensatory increase in electrical conductivity. Further investigation of these effects is planned.

Although the predicted total current density does not vary significantly with the GDL compression, the current density distribution changes noticeably. Fig. 11 shows that more current is produced under the channel area, because of the reduced oxygen diffusion in compressed region.

3.7. Reactant bypass phenomena

In a fuel cell flow-field plate with serpentine type channels, the reactant partial pressure as well as total pressure decreases along the flow path. Accordingly, there are certain locations in the flow-field plate where both the reactant partial pressure and total pressure in the adjacent flow-channels differ significantly. These conditions promote diffusive and/or convective transport of reactants through the GDL from one channel to a neighboring channel where partial and total pressure is lower. This phenomenon is often referred as reactant

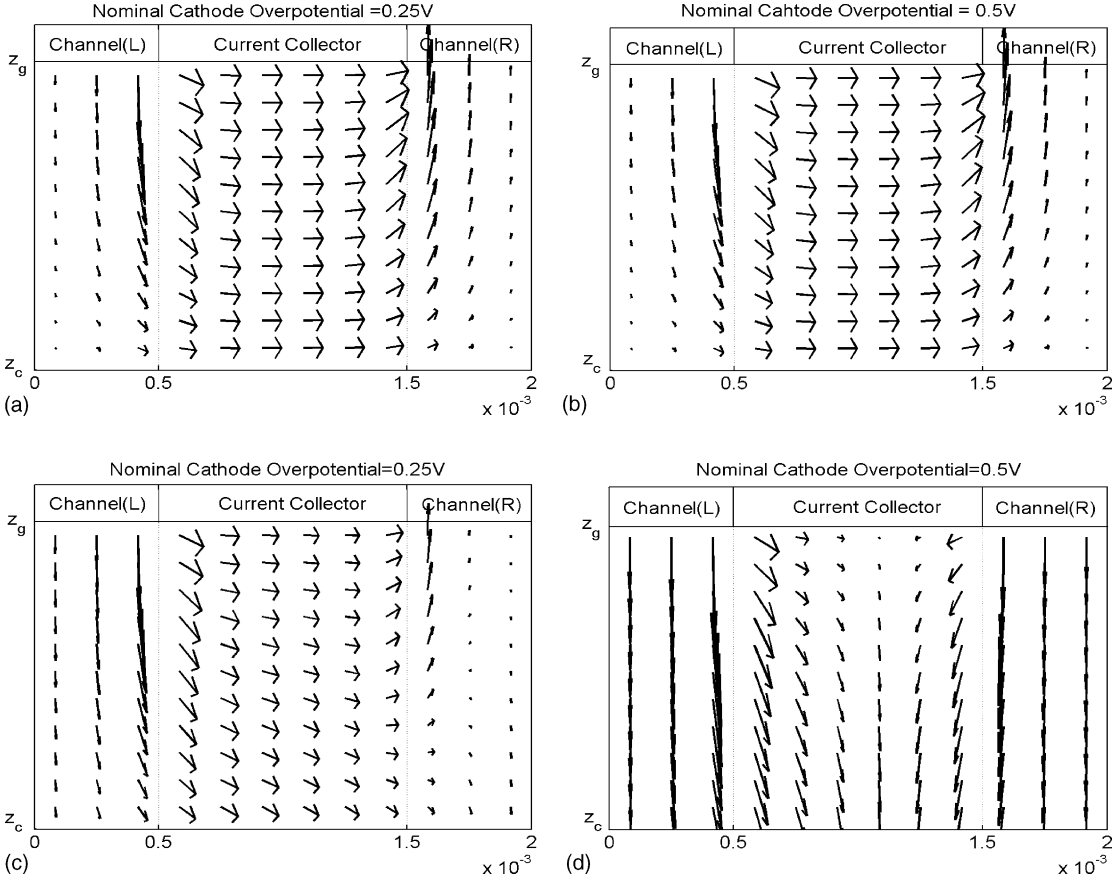

Fig. 12. Oxygen flux in the GDL. High permeability cases under NCOs: (a) 0.25 V and (b) 0.5 V. Low permeability cases under NCOs: (c) 0.25 V and (d) 0.5 V.

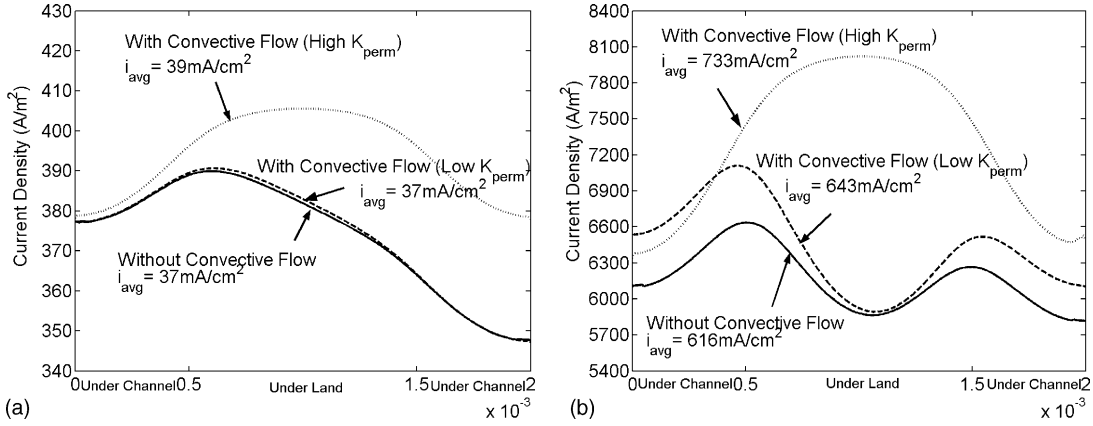

Fig. 13. The effect of convective flow between adjacent channels on current density distribution at the electrode–membrane interface. NCOs: (a) 0.25 V and (b) 0.5 V.

bypass [48]. Mench et al. [49] have suggested that this "undesired" reactant penetration may lead to dramatically reduced performance for fuel cell due to the reactant starvation. The two-dimensional cross-the-channel model was used to investigate the impact of reactant bypass on cathode performance.

The convective flow in the porous GDL between adjacent section of channel may be described by Darcy's law:

$$u = -\left(\frac{k_{\text{perm}}}{\mu}\right)\nabla P \tag{22}$$

where, u is the velocity of the convective flow, k_{perm} is the gas permeability in the porous media, μ is the gas dynamic viscosity, P is the local gas pressure.

The continuity equation can be described by the following equation:

$$\nabla \cdot (\rho u) = 0 \tag{23}$$

where, ρ is the local gas density.

Simulations were conducted for conditions where the total pressure and oxygen partial pressure in an adjacent channel were arbitrarily assigned to be 90% of those in the base case channel. This assumption may not necessarily represent a real condition; but, it allows us to investigate the importance of convective flow in the GDL. For all the simulations, the dynamic viscosity of gas, μ, was kept constant at 2×10^{-5} [Pa s]. While, because a wide range of gas permeability in GDL, k_{perm}, ranging from 10^{-11} to 10^{-19} m^2 has been reported in the literature, two permeability values, 2.3×10^{-11} [18] and 10^{-15} [m^2] were used to account for the effect of the parameter. In order to investigate the influence of the convective flow generated by total pressure difference between the neighboring channels on the cathode performance, we also simulated the case without the consideration of the convective flow, where only oxygen partial pressure difference between two channels was considered but the total pressure was assumed to be constant. This case can be treated as a special case where the gas permeability is equal to zero.

Fig. 12 shows the oxygen flux in the GDL for two different NCOs. When high gas permeability is used, as shown in the cases (a) and (b), there is significant oxygen flux from one channel to the other and towards the catalyst layer. This leads to an increase in oxygen concentration underneath the land area. For low gas permeability in the GDL, when the NCO is low (see Fig. 12c), a portion of the oxygen flux is also directed towards the adjacent channel. When the NCO increases, the driving force for oxygen transport to the catalyst layer may be higher than that for the transport of oxygen to the adjacent channel due to the total and partial pressure difference of oxygen. As such, there is no net oxygen flux between adjacent channels (see Fig. 12d).

To illustrate the effect of convective flow under the land, the predicted current density at $z = 0$ for both with and without convective flow are shown in Fig. 13. There is a significant enhancement in the electrochemical reaction under the land area for high permeability cases, indicating that the reactant bypass phenomenon is beneficial to cathode performance. For low permeability conditions the convective flow has smaller impact on the cathode performance, but the predicted current density is not reduced due to reactant bypass. Overall, the simulation results indicate that reactant bypass will have a positive effect on cathode performance contrary to previous published predictions [49].

4. Conclusions

The influence of geometric parameters and transport coefficients of the gas diffusion layer and flow-field plate on the cathode performance has been investigated using an improved two-dimensional electrode catalyst agglomerate model.

Simulations done to study the effect of channel-to-land width ratio indicate that increasing Ch-Ld ratio results in improved water transport and positively affects the overall oxygen reduction reaction rate at high overpotential. Simulation results using an improved model of the GDL indicate that

the transport for both gas and electrons plays an important role in cathode performance. Both the electronic conductivity and GDL thickness could be key parameters to be optimized to facilitate transport of electrons and chemical species. Differences between in- and through-plane conductivities in the GDL had a significant impact the reaction rate distribution in the catalyst layer.

The improved two-dimensional cross-the-channel model was further used to conduct preliminary studies of the effect of GDL compression and channel-to-channel reactant bypass. The simulation results indicate that moderate GDL compression does not significantly influence cathode performance for single-phase flow conditions. Moreover, channel-to-channel bypass flow under the land is predicted to have a positive impact on cathode performance.

Acknowledgements

The authors acknowledge the financial support from NSERC, CAMM, and DuPont Canada Inc., as well as the technical discussions with Dr. Jon Pharoah at Queen's University.

References

[1] EG&G Services, Parsons, Inc., Science Applications International Corporation, Fuel Cell Handbook, 5th ed., US Dept. of Energy, 2000.
[2] D.M. Bernardi, M.W. Verbrugge, AIChE J. 37 (8) (1991) 1151–1163.
[3] D.M. Bernardi, M.W. Verbrugge, J. Electrochem. Soc. 139 (9) (1992) 2477–2491.
[4] T.E. Springer, T.A. Zawodzinski, S. Gottesfeld, J. Electrochem. Soc. 138 (8) (1991) 2334–2342.
[5] G. Murgia, L. Pisani, M. Valentini, B. D'Aguanno, J. Electrochem. Soc. 149 (1) (2002) A31–A38.
[6] G.J.M. Janssen, J. Elctrochem. Soc. 148 (12) (2001) A1313–A1323.
[7] A. Rowe, X. Li, J. Power Sources 102 (2000) 82–96.
[8] T.F. Fuller, J. Newman, J. Electrochem. Soc. 140 (1993) 1218–1225.
[9] T.V. Nguyen, R.E. White, J. Electrochem. Soc. 140 (8) (1993) 2178–2186.
[10] V. Gurau, H. Liu, S. Kakac, AIChE J. 44 (11) (1998) 2410–2422.
[11] Z.H. Wang, C.Y. Wang, K.S. Chen, J. Power Sources 94 (2001) 40–50.
[12] A. Kazim, H.T. Liu, P. Forges, J. Appl. Electrochem. 29 (1999) 1409–1416.
[13] A.A. Kulikovsky, J. Divisek, A.A. Kornyshevb, J. Electrochem. Soc. 146 (11) (1999) 3981–3991.
[14] A.A. Kulikovsky, J. Appl. Electrochem. 30 (2000) 1005–1014.
[15] A.A. Kulikovsky, Electrochem. Commun. 3 (2001) 460–466.
[16] S. Dutta, S. Shimpalee, J.W. Van Zee, J. Appl. Electrochem. 30 (2) (2000) 135–146.
[17] T. Berning, D.M. Lu, N. Djilali, J. Power Sources 106 (2002) 284–294.
[18] T. Berning, N. Djilali, J. Electrochem. Soc. 150 (12) (2003) A1598–A1607.
[19] T. Berning, N. Djilali, J. Power Sources 124 (2003) 440–452.
[20] K.Z. Yao, K. Karan, K.B. McAuley, P. Oosthuizen, B. Peppley, T. Xie, Fuel Cells: Fundam. Syst. 4 (1–2) (2004) 3–29.
[21] A.C. West, T.F. Fuller, J. Appl. Electrochem. 26 (6) (1996) 557–565.
[22] T.E. Springer, M.S. Wilson, S. Gottesfeld, J. Electrochem. Soc. 140 (12) (1993) 3513–3526.
[23] C. Marr, X. Li, J. Power Sources 77 (1) (1999) 17–27.
[24] R.P. Iczkowski, M.B. Cutlip, J. Electrochem. Soc. 127 (1980) 1433–1440.
[25] S.J. Ridge, R.E. White, Y. Tsou, R.N. Beaver, G.A. Eisman, J. Electrochem. Soc. 136 (7) (1989) 1902–1909.
[26] F. Gloaguen, R. Durand, J. Appl. Electrochem. 27 (1997) 1029–1035.
[27] F. Gloaguen, P. Convert, S. Gamburzev, O.A. Velev, S. Srinivasan, Eletrochim. Acta 43 (24) (1998) 3767–3772.
[28] K. Broka, P. Ekdunge, J. Appl. Electrochem. 27 (1997) 281–289.
[29] F. Jaouen, G. Lindbergh, G. Sundholmb, J. Elctrochem. Soc. 149 (4) (2002) A437–A447.
[30] J. Ihonen, F. Jaouen, G. Lindbergh, A. Lundblad, G. Sundholmb, J. Elctrochem. Soc. 149 (4) (2002) A448–A454.
[31] K. Dannenberg, P. Ekdunge, G. Lindbergh, J. Appl. Electrochem. 30 (2000) 1377–1387.
[32] N.P. Siegel, M.W. Ellis, D.J. Nelson, M.R. Spakovsky, J. Power Sources 115 (2003) 81–89.
[33] W. Sun, B.A. Peppley, K. Karan, Electrochm. Acta, in preparation.
[34] W. Sun, MSc Thesis, Queen's University, Kingston, Ont., Canada, 2005.
[35] C. Curtiss, R. Bird, Ind. Eng. Chem. Res. 38 (1999) 2515–2522.
[36] D. Hamilton, M. Austin, J. Pharoah, Proceedings of the Hydrogen and Fuel Cells 2004 Conference and Trade Show, Toronto, Ont., Canada.
[37] A. Parthasarathy, S. Srinivasan, A.J. Appleby, C.R. Martin, J. Electrochem. Soc. 139 (10) (1992) 2856–2862.
[38] H.S. Fogler, Elements of Chemical Reaction Engineering, Prentice-Hall, New Jersey, 1999.
[39] Comsol, Inc, FEMLAB User's Guide and Introduction, Version 2.2, 2001.
[40] S.J. Lee, S. Mukerjee, J. McBreen, Y.T. Rho, T.H. Lee, Eletrochim. Acta 43 (24) (1998) 3693–3701.
[41] J. Kim, S. Lee, S. Srinivasan, C.E. Chamberlin, J. Electrochem. Soc. 142 (8) (1995) 2670–2674.
[42] J.C. Amphlett, R.M. Baumert, R.F. Mann, B.A. Peppley, P.R. Roberge, T.J. Harris, J. Electrochem. Soc. 142 (1) (1995) 1–8.
[43] J.C. Amphlett, R.M. Baumert, R.F. Mann, B.A. Peppley, P.R. Roberge, T.J. Harris, J. Electrochem. Soc. 142 (1) (1995) 9–15.
[44] M. Bang, S. Yde-Anderson, T. Condra, N. Djilali, E. Skou, Proceedings of the Hydrogen and Fuel Cells 2003 Conference, Vancouver, BC, Canada.
[45] B. Hum, X. Li, J. Appl. Electrochem. 34 (2004) 205–215.
[46] http://www.torayca.com/properties/en/images/report_eng09_2.html (retrieved date: November 20, 2004).
[47] http://www.ballard.com/resources/carbon_fiber/AvCarbCFP.pdf (retrieved date: November 20, 2004).
[48] S. Um, C.Y. Wang, Proceedings of the ASME Heat Transfer Division, 2000, HTD-366-1, pp. 19–25.
[49] M.M. Mench, C.Y. Wang, S. Thynell, Int. J. Transport Phenom. 3 (2001) 151–176.
[50] A. Parthasarathy, S. Srinivasan, A.J. Appleby, C.R. Martin, J. Electrochem. Soc. 139 (9) (1992) 2530–2537.
[51] G. Li, P.G. Pickup, J. Electrochem. Soc. 150 (11) (2003) C745–C752.
[52] R.B. Bird, W.E. Stewart, E.N. Lightfoot, Transport Phenomena, Wiley, New York, 1960.
[53] A. Fisher, J. Jindra, H. Wendt, J. Appl. Electrochem. 28 (1998) 277–282.